

# Adsorption of Poly(amidoamine) Dendrimers on Gold

K. M. A. Rahman, C. J. Durning,\* N. J. Turro, and D. A. Tomalia

Department of Chemical Engineering and Applied Chemistry, Columbia University,  
New York, New York 10027

Received September 28, 1999. In Final Form: April 18, 2000

Adsorption of poly(amidoamine) (PAMAM) dendrimers from dilute solution onto cleaned gold has been studied *in-situ* by a quartz crystal microbalance technique. All experiments were carried out at 21 °C, with either anhydrous ethanol or deionized water as solvent. In ethanol, the equilibrium frequency shifts, proportional to the equilibrium surface coverages,  $\Gamma$  [ $M/L^2$ ], correspond to about a monolayer and increase weakly (roughly linearly) with generation,  $G$ . The adsorption is likely driven by the weak favorable interaction between the primary amine end groups on PAMAM and gold. In aqueous media, the results are completely different. Under the conditions employed (low ionic strength and pH 6.5–7) the PAMAM amine end groups tend to protonate in aqueous solution, so that the macromolecules bear positive charge. The equilibrium frequency shift grows exponentially with generation  $G$  up to  $G = 6$ . For  $G = 7$  a drastic drop is observed, but the increasing trend resumes again for  $G = 7$  through  $G = 9$ . Estimates of the adsorbed layer thickness indicate that multilayers form on the clean gold surface in the aqueous system with the number of layers increasing exponentially up to  $G = 6$ . The formation of multilayers can be explained by a favorable electrostatic image–charge interaction between the positively charged dendrimers in aqueous solution and the gold substrate. By accounting for charge renormalization and screening, this picture quantitatively accounts for the dependence of  $\Gamma$  on  $G$ , for  $G \leq 6$ . The drop in frequency shift from  $G = 6$  to  $G = 7$  may be the result of surface crowding discussed in connection with the “dense-shell” transition of the dendrimer external surface.

## I. Introduction

Dendrimers are highly branched, nearly monodisperse polymers possessing a well-defined molecular architecture. Their structure is characterized by three distinct features: (i) a central multifunctional core, (ii) tiers or “generations” of multifunctional repeat units attached around the core, and (iii) terminal or end groups. Manipulating these structural features allows controlled synthesis of a whole series of highly branched, end-functionalized macromolecules that are drawing increasing attention for many potential applications, including magnetic resonance imaging contrast agents,<sup>1,2</sup> immunoassays,<sup>3</sup> drug delivery systems,<sup>4,5</sup> DNA complexation,<sup>6</sup> sensors<sup>7</sup> and catalysts.<sup>8</sup> The potential for surface modification with dendrimers is tremendous. In particular, dendrimers may provide a viable alternative to surface modification by self-assembled monolayers (SAMs) of linear species.<sup>9–14</sup> SAMs prepared from linear alkyl or aromatic chains have limited surface stability due to

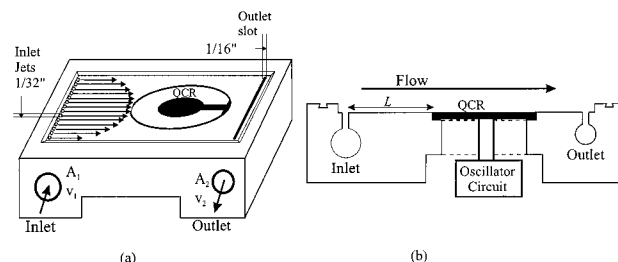


**Figure 1.** (a) Schematic view of the flow-cell base. (b) Cross-sectional view.

monopodial surface attachment. Dendrimer monolayers or multilayers could offer an attractive alternative, because they possess a large number of end groups per molecule and thereby improved surface functionality, as well as excellent adhesion to surfaces and thereby improved stability.

In this work we study adsorption onto gold from dilute alcoholic and aqueous solutions of poly(amido amine) (PAMAM) dendrimers in order to determine their potential for surface modification. For PAMAMs, the core can be either a trifunctional amine or a tetrafunctional ethylenediamine (EDA) molecule. The end or “surface” groups for “full generation” PAMAM dendrimers are primary amines, so that two additional repeat units can be attached per end group. Thus, for the EDA core PAMAM dendrimers used in this work, the total number of primary amine end groups for generation  $G$  is  $2^{(G+2)}$ .

\* Corresponding author. Phone: (212) 854-8161. Fax: (212) 854-3054. E-mail: cjd2@columbia.edu.

(1) Weiner, E. C.; Brechbiel, M. W.; Brothers, H.; Magin, R. L.; Gansow, O. A.; Tomalia, D. A.; Lauterbur, P. C. *Magn. Reson. Med.* **1994**, *31* (1), 1–8.

(2) Toth, E.; Pubanz, D.; Vauthey, S.; Helm, L.; Merbach, A. E. *Chem.-Eur. J.* **1996**, *2* (12), 1607–1615.

(3) Singh, P.; Moll, F.; Lin, S. H.; Ferzli, C.; Yu, K. S.; Koski, R. K.; Saul, R. G. *Cronin, P. Clin. Chem.* **1994**, *40* (9), 1845–1849.

(4) Beezer, A. E.; Mitchell, J. C.; Colegate, R. M.; Scally, D. J.; Twyman, L. J.; Willson, R. J. *Thermochim. Acta.* **1995**, *250* (2), 277–283.

(5) Twyman, L. J.; Beezer, A. E.; Esfand, R.; Hardy, M. J.; Mitchell, J. C. *Tetrahedron Lett.* **1999**, *40* (9), 1743–1746.

(6) Bielinska, A. U.; KukowskaLatalo, J. F.; Baker, J. R. *Biochim. Biophys. Acta-Gene Struct. Expr.* **1997**, *1353* (2), 180–190.

(7) Albrecht, M.; Gossage, R. A.; Speck, A. L.; van Koten, G. *Chem. Commun.* **1998**, Iss 9, 1003–1004.

(8) Gossage, R. A.; Jastrzebski, J. T. B. H.; van Ameijde, J.; Mulders, S. J. E.; Brouwer, A. J.; Liskamp, R. M. J.; van Koten, G. *Tetrahedron Lett.* **1999**, *40* (7), 1413–1416.

(9) Caminade, A. M.; Laurent, R.; Chaudret, B.; Majoral, J. P. *Coord. Chem. Rev.* **1998**, *180*, 793–821.

(10) Balogh, L.; de Leuze-Jallouli, A.; Dvornic, P.; Kunugi, Y. T.; Blumstein, A.; Tomalia, D. A. *Macromolecules* **1999**, *32* (4), 1036–1042.

(11) Iyer, J.; Hammond, P. T. *Langmuir* **1999**, *15* (4), 1299–1306.

(12) Schlenk, C.; Frey, H. *Monatsh. Chem.* **1999**, *130* (1), 3–14.

(13) Hierlemann, A.; Campbell, J. K.; Baker, L. A.; Crooks, R. M.; Ricco, A. J. *J. Am. Chem. Soc.* **1998**, *120*, 5323–5324.

(14) Tokuhisa, H.; Zhao, M. Q.; Baker, L. A.; Phan, V. T.; Dermody, D. L.; Garcia, M. E.; Peez, R. F.; Crooks, R. M.; Mayer, T. M. *J. Am. Chem. Soc.* **1998**, *120*, 4492–4501.

It is known that primary amines in aqueous solution are protonated<sup>15</sup> at  $\text{pH} \leq 8$  so that the PAMAM dendrimers bear a predictable structural charge in aqueous solution under these conditions. By contrast, primary amines remain uncharged at higher pH or in low molecular weight alcohols (e.g. ethanol). By comparing results for PAMAM adsorption onto gold from low pH aqueous and alcoholic media, one assesses the role of electrostatic forces in the formation of PAMAM adsorbed layers.

In what follows, we first discuss our technique, utilizing a quartz crystal resonator (QCR) for measuring surface coverage *in-situ* on clean gold surfaces from gently flowing solution. Then we present a systematic study of the adsorption of full generation EDA core PAMAM dendrimers from dilute aqueous solution at low ionic strength and pH. The data indicate formation of thick multilayers on gold for  $G$  up to 6, because of an induced electrostatic interaction between the charged macromolecules and the conducting surface. Surprisingly, an abrupt transition in coverage,  $\Gamma$  [ $M/L^2$ ], with generation,  $G$ , occurs at  $G = 6$ , which may indicate the threshold for surface congestion associated with a “dense-shell” transition.<sup>16</sup> Following that, we summarize results for adsorption from ethanolic solutions. The data differ dramatically from the case of aqueous media; neither multilayer adsorption nor the abrupt transition in coverage at  $G = 7$  occurs. Instead, simple monolayer formation is seen for all generations. The results suggest that one can manipulate the coverage of PAMAMs on gold significantly, from monolayers to multilayers, by altering the solution conditions to manipulate the role of electrostatic forces.

## II. Experimental Section

**A. Quartz Crystal Microbalance.** To monitor adsorption *in-situ*, we employ thickness-shear-mode piezoelectric transducers made from flat, “AT” cut  $\alpha$ -quartz plates<sup>17</sup> with concentric circular gold electrodes evaporated onto opposing surfaces. Alternating current excitation causes periodic shear deformation of the plate with shear planes parallel to the plate surface; the motion corresponds to propagation of a transverse shear wave normal to the plate. Such plates are frequently called quartz crystal resonators (QCRs) because of their sharply defined resonances. These correspond to the surfaces being out-of-phase antinodes of motion; that is, the resonance frequencies,  $f_n$ , are where  $(n)/(2)\lambda$ ,  $n = 1, 3, 5, \dots$ , matches the plate thickness  $l_q$ , where  $\lambda = \sqrt{\mu_q/\rho_q} f_n^{-1}$ , the shear wavelength in quartz. Consequently,

$$f_n = \frac{n}{2l_q} \sqrt{\frac{\mu_q}{\rho_q}}, \quad n = 1, 3, 5, \dots \quad (1)$$

where  $\mu_q$  and  $\rho_q$  are the elastic modulus<sup>18</sup> and the density of quartz, respectively.

When a QCR is put in a properly designed feedback oscillator circuit, the circuit will oscillate near the lowest mode resonance frequency ( $n = 1$ ) of the quartz plate. One can monitor the frequency of such a circuit to track changes in the resonance frequency due to interfacial interaction between the plate surface and its environment. Adsorption of a thin layer onto the surface results in an increase in the effective mass of the plate. Contacting the QCR with a viscous liquid increases the damping on the oscillating plate. Both effects cause a *decrease* in the resonance frequency.

When a thin layer is deposited onto an unloaded QCR, the observed resonance frequency shift due to the increase in the plate's inertia is given by

$$\Delta f_M = -a\beta\Gamma \quad (2)$$

where  $\Gamma$  is the areal density of the adsorbed layer, that is, the surface coverage [ $M/L^2$ ]. Also,  $a = 2\pi f_1$  [ $T^{-1}$ ] is the angular resonant frequency of the unloaded plate and  $\beta = f_1/\pi Z_q$  [ $L^2/M$ ], with  $Z_q = \sqrt{\mu_q \rho_q}$  being the acoustic impedance of quartz. Equation 2, first derived by Sauerbrey,<sup>19</sup> is the basis of the “quartz crystal microbalance”: the oscillator frequency shift reports the mass per unit area of a deposited layer. In practice one finds the “sensitivity”  $\beta$  is an instrument constant varying somewhat with the fixtures and feedback circuit used.

Loading a resonating crystal with a viscous liquid also results in a frequency shift, due to the damping. For hydrodynamically smooth crystals, it is given by<sup>20</sup>

$$\Delta f_D = -b\beta(\rho\eta)^{1/2} \quad (3)$$

where  $b = a/2(f_1/\pi)^{1/2}$  [ $T^{-1/2}$ ]. When both mass deposition and viscous damping occur simultaneously, shifts 2 and 3 are superposed. An additional contribution,  $\Delta f_X$ , arises with liquid contact from nonshear (i.e., acoustic) coupling between a damping liquid and the oscillating crystal. This depends on surface roughness<sup>21</sup> and is proportional to the fluid density,  $\rho$ . Consequently, the total frequency shift for simultaneous adsorption and damping from a liquid is of the form

$$\Delta f_T = \Delta f_M + \Delta f_D + \Delta f_X = -\beta[a\Gamma + b'(\rho\eta)^{1/2} + c\rho] \quad (4)$$

with  $a'/b' = a/b = 2(\pi f_1)^{1/2}$ . Equation 4 provides a basis for quantitative analysis of frequency shifts for the surface coverage,  $\Gamma$ , after calibration to determine  $\beta a'$ .

**B. Flow-Cell System.** We designed and built a Hele-Shaw flow-cell for liquid-phase QCR measurements. The cell allows flush-mounting of a QCR at a position in a flat channel where fully developed laminar flow exists. Figure 1a shows a schematic. The entrance length needed for fully developed flow,  $L$  (Figure 1b), was calculated<sup>22</sup> for viscous liquids with viscosities up to  $\sim 100$  cps. A fluorosilicon-based glue seals the QCR in position. The glue is impervious to aqueous and many organic liquids, including ethanol, and ensures a proper seal. Being flush-mounted on a precisely machined groove, the crystal can function under nearly stress-free conditions.

Overtone polished, 1 in. diameter quartz crystals (Maxtek, Inc., Torrance, CA) with the upper electrode area 1.27  $\text{cm}^2$  and nominal resonance frequency 5 MHz were used. The surface roughness of as-received crystals was measured by AFM; the typical rms value was found to be  $\approx 30$  Å. Prior to their use the crystals were first rinsed with deionized water and then immersed in “piranha solution” (1:3 v/v 30%  $\text{H}_2\text{O}/\text{H}_2\text{SO}_4$ ) for  $\approx 5$  min at room temperature. The crystals were then rinsed thoroughly in running deionized water and dried with a moderate flow of filtered dry  $\text{N}_2$  gas. A feedback oscillator circuit (Maxtek, Inc., Torrance, CA) is placed just beneath the QCR, minimizing stray-capacitance and inductance. The working (upper) electrode of the QCR is maintained at ground potential while a small amplitude ( $\sim 300$  mV) ac signal is applied to the bottom electrode. A controller (model PI-70, Maxtek, Inc., Torrance, CA) drives the oscillator circuit and reports the resonance frequency of the QCR to a frequency counter (HP 5384A) in real time.

Figure 2 shows the experimental arrangement utilizing this flow-cell. The flow system consists of a reservoir, a magnetic gear pump (Micropump model # 120-000-110, Cole-Parmer, Chicago, IL), and the Hele-Shaw cell described above connected by inert tubing. The entire flow-circuit has a dead volume of  $\sim 30$  mL. The setup is enclosed inside a stainless steel Faraday cage.

(15) Tomalia, D. A.; Naylor, A. M.; Goddard, W. A., III. *Angew. Chem., Int. Ed. Engl.* **1990**, *29*, 138–175.

(16) de Gennes, P. G.; Hervet, H. *J. Phys. Lett.* **1983**, *44*, L351–360.

(17) The cut refers to the orientation of the crystal unit cell with respect to the plane of the plate; the designations AT, BT, and SC are three different orientations which can result in thickness–shear mode resonators.

(18) The modulus in eq 1 is a particular combination of the elastic constants characterizing the  $\alpha$ -quartz unit cell.

(19) Sauerbrey, G. *Z. Phys.* **1959**, *155*, 206.

(20) Kanazawa, K. K.; Gordon, J. G. *Anal. Chem.* **1985**, *57*, 1770. Kanazawa, K. K.; Gordon, J. G. *Anal. Chem. Acta* **1985**, *175*, 99.

(21) Yang, M.; Thompson, M. *Langmuir* **1993**, *9*, 802.

(22) Fox, R. W.; McDonald, A. *Introduction to Fluid Mechanics*, 2nd ed.; Wiley: New York, 1978.

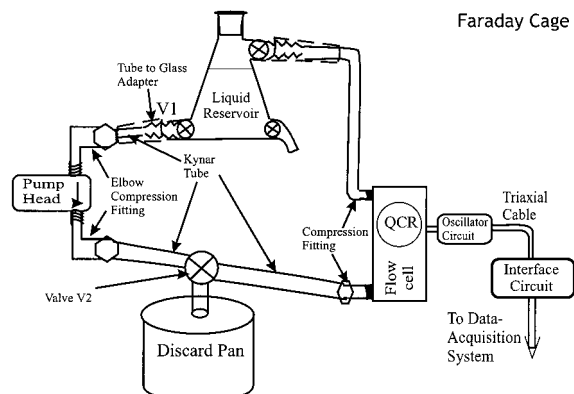


**Figure 2.** Schematic of experimental setup.

A PC equipped with an HP-IB data acquisition card (HP 82335B) acquires the frequency versus time data.

The experimental protocol for monitoring adsorption from solution *in-situ* is as follows. The QCR is first equilibrated against air and then against pure solvent. The flowing solvent is then exchanged with solution containing the adsorbate. Frequency shifts observed thereafter, denoted  $\Delta f$ , are solely due to the adsorption of macromolecules from the solution onto the upper QCR electrode. All measurements reported subsequently were done at room temperature at the flow rate  $3.5 \text{ cm}^3/\text{s}$ . The calibration procedure discussed by Pan et al.<sup>23</sup> was used to establish a quantitative relationship between the resonance frequency shift,  $\Delta f$ , and the surface coverage,  $\Gamma$ . This protocol has been proven accurate to within  $\pm 10\%$  in electrodeposition experiments where  $\Gamma$  was measured independently by electrochemical means.<sup>24</sup>

**C. Materials.** After calibration, the setup was used for quantitative determination of the surface coverage of poly-(amidoamine) (PAMAM) dendrimers on gold surfaces from aqueous solution and ethanolic solution. EDA core PAMAM dendrimers, synthesized by one of us, were prepared by the following process.<sup>26</sup> The first step is an exhaustive Michael addition of methyl acrylate to an ethylenediamine (EDA) initiator core. Then an exhaustive amidation of the resulting ester is carried out with a large excess of ethylenediamine. This produces PAMAM dendrimer of "generation"  $G = 0$ . Higher generation analogues were prepared by repetition of the Michael addition and amidation steps. Note that in aqueous solution at pH below 8 the terminal amines are expected to be protonated,<sup>15</sup> which is the case in the present study. Thus, strong electrostatic interactions are expected in this system. On the other hand, no such protonation is expected for the solutions in ethanol.<sup>25</sup> Consequently, relatively weak, short-ranged dispersive forces or permanent dipole interactions govern adsorption in this case.

Samples of generation  $1 \leq G \leq 9$  were prepared as concentrated stock solutions either in methanol or in water. To prepare dilute aqueous solutions for adsorption studies from stock solutions in methanol, the required volume of the stock (typically  $200\text{--}300 \mu\text{L}$ ) was first dried in a vacuum oven under a moderate vacuum and mild heating ( $\leq 80 \text{ }^\circ\text{C}$ ) before adding water as solvent. Typically it took  $2\text{--}3 \text{ h}$  to dry completely. Prior experience with PAMAM dendrimer synthesis indicates that these drying conditions do not result in degradation (i.e. reverse Micheal reaction).<sup>27</sup> Samples supplied as aqueous stock solutions were used as received. To prepare solutions in ethanol, the required volume of stock solution was evaporated as described above and the dilute solution was formed by adding ethanol.

All aqueous solutions for adsorption were prepared in nominally  $18 \text{ M}\Omega$  deionized water at the polymer concentration  $100 \mu\text{g}/\text{mL}$ . The resulting pH values were found to be within  $6.5\text{--}7$

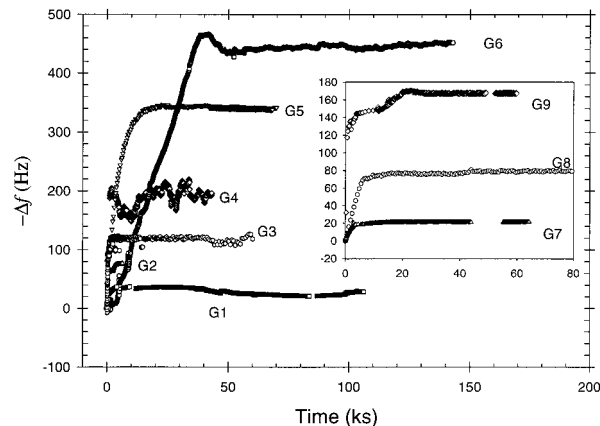


**Figure 3.** Frequency shifts during dendrimer adsorption on gold from aqueous solution.

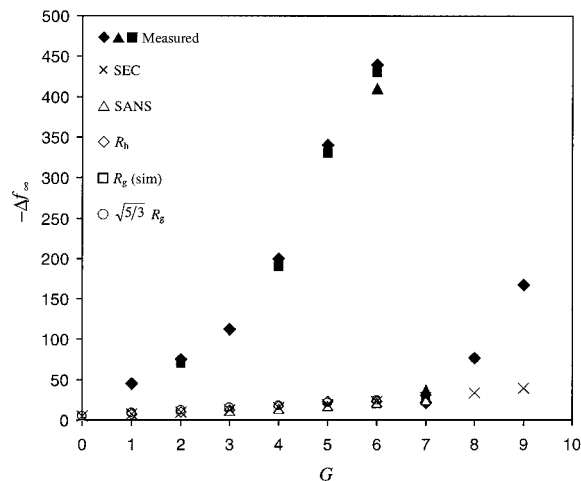


**Figure 4.** Equilibrium frequency shifts,  $-\Delta f_\infty$  versus generation  $G$  for PAMAM dendrimers adsorbed from aqueous solution ( $\blacklozenge$ ,  $\blacktriangle$ ,  $\blacksquare$ ). Also shown are  $-\Delta f_\infty$  versus  $G$  predicted for close-packed monolayer of spheres using eq 5: ( $\times$ ) from eq 5 with  $r_S$  from size exclusion chromatography;<sup>37</sup> ( $\diamond$ ) from eq 5 with  $r_S$  from small angle neutron scattering;<sup>29</sup> ( $\triangle$ ) from eq 5 with  $r_S$  from hydrodynamic radii;<sup>29</sup> ( $\square$ ) from eq 5 with  $r_S$  from radii of gyration,  $R_g$ , obtained from simulation via energy minimization (see text); ( $\circ$ ) from eq 5 with  $r_S$  from geometric radii calculated from  $R_g$  obtained from simulation.

as measured with a pH meter (Corning model 150). All solutions in ethanol were prepared using reagent grade anhydrous ethanol (Aldrich, Milwaukee, WI) at the concentration  $100 \mu\text{g}/\text{mL}$ . No special precautions were taken to exclude ambient moisture from these solutions.

### III. Results and Discussion

We measured the frequency shifts due to adsorption of dendrimers,  $\Delta f$ , for generations  $G = 1$  to  $G = 9$  in aqueous solution and for  $G = 2, 5, 7,$  and  $9$  in ethanolic solution. For several generations, the adsorption experiments were repeated a few times using independently synthesized lots of polymer.

**A. Adsorption from Aqueous Solution.** Figure 3 displays representative data of the frequency shift,  $\Delta f$ , versus time  $t$  after introducing aqueous dendrimer solution in the flow-cell, for generations 1 through 9. The equilibrium frequency shifts due to adsorption,  $\Delta f_\infty$ , are shown in Figure 4 for all the runs performed. Each filled symbol in Figure 4 corresponds to a single run in the flow cell. The uncertainty in the  $\Delta f_\infty$  for individual runs was

(23) Pan, W.; Durning, C. J.; Turro, N. J. *1996*, *12*, 4469–4473.

(24) Kelly, J. J.; Rahman, K. M. A.; Durning, C. J.; West, A. C. *J. Electrochem. Soc.* **1998**, *145*, 492–497.

(25) Fuoss, R. M.; Kraus, C. A. *J. Am. Chem. Soc.* **1933**, *55*, 1019.

(26) Tomalia, D. A.; Baker, H.; Dewald, J.; Hall, M.; Kallos, G.; Martin, S.; Roeck, J.; Ryder, J.; Smith, P. *Macromolecules* **1986**, *19*, 2466–4510.

(27) Balogh, L. University of Michigan, private communication.

determined by fluctuations in the  $t \leq 0$  and  $t \gg 0$  baselines and is on the order of the size of the symbols in Figure 4 ( $\pm 15$  Hz). Repeatability, indicated by multiple data points for several generations in Figure 4, was within 15%.

From Figure 4 one can see that  $\Delta f_\infty$  increases very rapidly as a function of generation up to  $G = 6$ , while, for  $G = 7$ , it exhibits an unusual drop. For  $G = 7$  through  $G = 9$ , the strongly increasing trend resumes. To check the reproducibility of the drop from  $G = 6$  to  $G = 7$ , we repeated measurements at these generations with samples from different batches of polymer, prepared from both aqueous and methanolic stocks.

**1. Monolayer Models.** It has been reported<sup>13,14</sup> and confirmed by us in this work (see later) that PAMAM dendrimers form monolayers on gold when deposited from ethanolic solution. Consequently, one might naively expect monolayer formation for adsorption from aqueous media even though the macromolecules bear charge. If the adsorbing molecules retain their (roughly) spherical shape and form a close packed monolayer, then the surface coverage would be

$$\Gamma = \frac{\text{mass}}{\text{projected area}} \approx \frac{4\rho r_S}{3} \quad (5)$$

where  $r_S$  is the radius of the dendrimer and  $\rho$  is its total internal density. From eq 5 and the calibration constants for the flow cell connecting  $\Delta f$  and  $\Gamma$ , one can predict  $\Delta f_\infty$  for monolayer coverage, using literature values of  $r_S$  for PAMAMs and assuming  $\rho \approx 1 \text{ g/cm}^3$ . Figure 4 shows  $\Delta f_\infty$  versus  $G$  predicted in this way (open symbols) along with the measured data for aqueous solutions (filled symbols). For the predictions, several sets of  $r_S$  values were used, as indicated in the caption, including a set of radii of gyration,  $R_g$ , obtained by us from molecular modeling using commercial molecular simulation software (Cerius2 from MSI Inc.). Here, the  $R_g$  values were calculated from time averages computed during molecular dynamics runs using an energy minimized configuration as an initial state. The initial configurations were obtained using a CFF91 force-field.<sup>28</sup> The subsequent molecular dynamics were run at constant volume and the temperature 300 K for  $\approx 25$  ps. From Figure 4 it is clear that a monolayer model of closely packed spheres cannot explain the observed behavior in aqueous solution except for generation  $G = 7$ . For the remaining samples it underpredicts the coverage, and completely misses the strongly increasing trend for  $G = 1$  through  $G = 6$ , as well as the abrupt change at  $G = 7$ .

Literature indicates that lower generations of dendrimers are flexible but that they show decreasing flexibility as  $G$  increases.<sup>16,29,30</sup> Consequently, a possible scenario is that, for low generations, monolayers form but with significant lateral compression of individual molecules until, at sufficiently high  $G$ , they can no longer tolerate the lateral squeezing and return to a more or less spherical shape and much lower surface coverage. To check this idea, we considered a monolayer of laterally compressed dendrimers, elongated into cylinders pointing normal to the surface. The coverage would then be given by

$$\Gamma = \frac{\text{mass}}{\text{projected area}} \approx \rho h \quad (6)$$

with  $h$  being the cylinder height. Assuming each molecule preserves its total volume and total internal density ( $\approx 1$

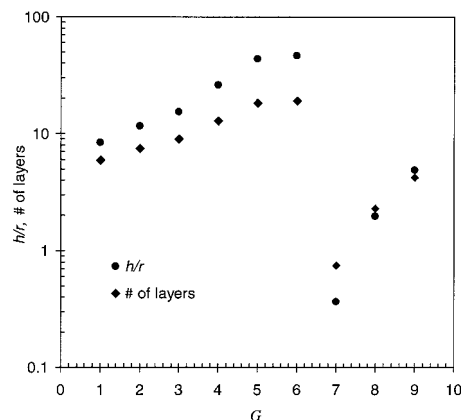


**Figure 5.** Aspect ratio ( $h/r$ ) for monolayer of cylindrical molecules assuming a fixed volume per molecule and density near  $1 \text{ g/cm}^3$  (●) and number of layers in a multilayer assuming density near  $1 \text{ g/cm}^3$  and spherical molecules with the radius reported in ref 37 (◆).

$\text{g/cm}^3$ ), one can calculate the radius of the cylinder after determining the height,  $h$ , from eq 6 and the measured  $\Delta f_\infty$  values. Figure 5 displays a semilog plot of the hypothetical aspect ratio  $h/r$ . The calculation indicates ratios approaching  $\approx 50$  for  $G = 6$ , which is clearly unrealistic. Thus, under the present experimental conditions one is led to conclude that multilayers form, except, of course, for  $G = 7$ .

One can estimate from the  $\Delta f_\infty$  data the thickness of the multilayer assuming the adsorbed layer density  $\approx 1 \text{ g/cm}^3$ . The corresponding number of layers follows from the dendrimer radii  $r_S$  assuming the adsorbed molecules remain roughly spherical. Figure 5 shows the number of layers estimated in this way; on the order of a dozen layers apparently form from aqueous solution for  $G = 5$  and  $G = 6$ .

**2. Mechanism of Multilayer Formation in Aqueous Media.** Because the dendrimers under consideration bear positive charge in aqueous solution at the conditions used, there exists an attractive image-charge interaction between the macroions in solution and the gold upper electrode at ground potential. We believe this effect causes the development of multilayers. If the macroions are treated as pointlike, the unscreened image-charge interaction energy,  $E$ , of a single polymer of charge  $Ze$  a distance  $d$  from a grounded upper electrode is

$$E = -\frac{(Ze)^2}{\epsilon} \frac{1}{2d} \quad (7)$$

in cgs units, where  $\epsilon$  is the dielectric constant of the medium containing the charge,  $Z$  is the structural charge on the macromolecule, and  $e$  is the protonic charge (see Figure 6). Since the number of surface groups for generation  $G$  of EDA core PAMAM dendrimers is  $2^{(G+2)}$  and, at the pH of our aqueous solutions, the surface groups (primary amines) are protonated<sup>15,31,32</sup> while the internal tertiary amines are not, the total structural charge per molecule is  $Z \approx 2^{(G+2)}$ . The characteristic adsorbed layer thickness,  $d^*$ , will be the distance for which the interaction

(29) Uppuluri, S.; Keinath, S. E.; Tomalia, D. A.; Dvornic, P. R. *Macromolecules* **1998**, *31*, 4498–4510.

(30) Jackson, C. L.; Chanzy, H. D.; Booy, F. P.; Drake, B. J.; Tomalia, D. A.; Bauer, B. J.; Amis, E. J. *Macromolecules* **1998**, *31* (18), 6259–6265.

(31) van Duijvenbode, R. C.; Borkovec, M.; Koper, G. J. M. *Polymer* **1998**, *39*, 2657.

(32) Ottaviani, M. F.; Montalti, F.; Turro, N. J.; Tomalia, D. A. *J. Phys. Chem. B* **1997**, *101*, 158.

(28) Maple, J. R.; Dinur, U.; Hagler, A. T. *Proc. Natl. Acad. Sci. U.S.A.* **1988**, *85*, 5350–5354.

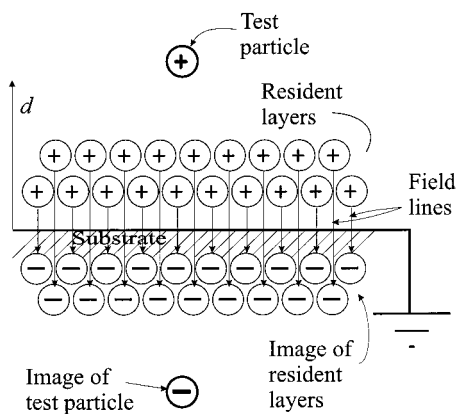


**Figure 6.** Schematic representation of the charged dendrimer layers and their images and the resulting electric field.

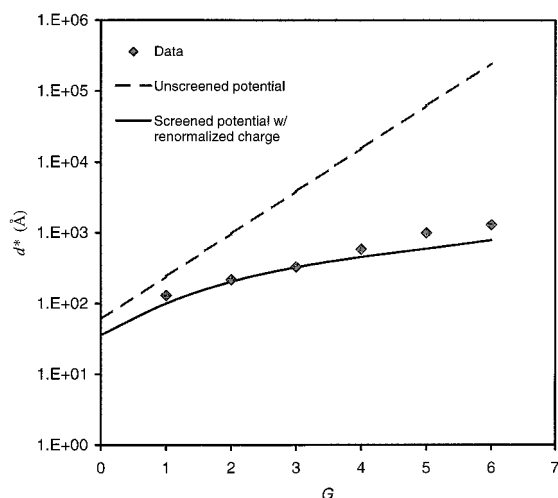


**Figure 7.** Thickness of adsorbed layers: (◆) calculate from measured frequency shift; (---) predicted by unscreened image–charge potential; (—) predicted by screened potential with renormalized charge.

energy falls to a value  $\sim kT$ . Consequently,

$$d^* \approx \frac{(Ze)^2}{2\epsilon kT} = \frac{Z^2 \lambda}{2} \quad (8)$$

where  $\lambda = e^2/\epsilon kT$  is the Bjerrum length (7 Å in water).

One may ask how the development of a nascent multilayer structure affects this interaction. Since the electric field lines associated with adsorbed macroions run almost directly toward their images, one does not expect the field lines to extend much beyond a resident layer (see Figure 6). Therefore, a “test” polymer approaching layers already in place would not “see” a strong repulsive field until very near the layer. At larger distances it should only experience the attractive interaction with its own image–charge. Therefore, it seems reasonable to use a pair interaction potential to estimate the ultimate thickness of the adsorbed multilayer.

Figure 7 shows  $d^*$  for generations 0 through 6 estimated from eq 8 assuming  $Z = 2^{G+2}$  and  $\epsilon$  with the value for water. Equation 8 clearly overestimates the exponential rate of increase in layer thickness with  $G$ . Several factors could be responsible for this. In our view, the most important are the effects of electrostatic screening and that the effective charge on the macromolecules could differ from  $2^{G+2}$ . We accounted for these two factors within the framework of the Poisson–Boltzmann theory for dilute

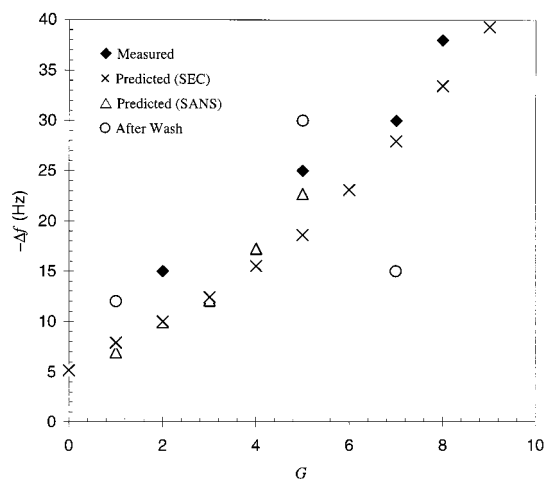


**Figure 8.** Equilibrium frequency shifts,  $-\Delta f_{\infty}$ , versus generation,  $G$ , for PAMAM dendrimers adsorbed from ethanol (◆) and for dendrimers adsorbed from aqueous solution after washing with pure 18 MΩ water (○). Also shown are  $-\Delta f_{\infty}$  versus  $G$  predicted from eq 5 with  $r_S$  from size exclusion chromatography (×)<sup>37</sup> and predicted from eq 5 with  $r_S$  from hydrodynamic radii (Δ).<sup>29</sup>

solutions of macroions with monovalent counterions and without added electrolyte.

According to ref 33 a good approximation to the pair interaction potential has the form

$$\phi(r) = -\frac{Z^* e e^{-\kappa r}}{\epsilon r} \quad (9)$$

where  $\kappa^{-1}$  is the effective Debye screening length given by

$$\kappa^2 = 4\pi Z^* c \lambda \quad (10)$$

Here,  $c$  is the macroion (i.e., dendrimer) concentration and  $Z^*$  is its effective, renormalized charge. We took  $c$  to be the bulk concentration of dendrimers in solution and calculated  $Z^*$  using the procedure recommended by Alexander et al.<sup>33</sup> (see Appendix). We estimate the layer thickness by comparing the screened electrostatic image–charge interaction energy with  $kT$ , which leads to

$$\ln(Z^{*2} \lambda) = \ln(2d^*) + \kappa^2 d^* \quad (11)$$

a transcendental equation which was solved for  $d^*$  numerically for each generation after finding  $Z^*$  and  $\kappa$  by the method described in the Appendix. Figure 7 shows the  $d^*$  values estimated from the screened potential with renormalized charge. The screened potential produces a reasonably good prediction of the apparent layer thickness with  $G$ , supporting the hypothesis of an image–charge mechanism driving the adsorption from aqueous solution. This view is supported further by the very different adsorption behavior observed for solutions in ethanol, where the dendrimers are uncharged and multilayers do not form (see later section).

Interestingly, it was found that the multilayers are bound rather weakly to the surface. This was assessed in “washing” experiments, where after equilibration we exchanged the flowing dendrimer solution with pure water flowing at the same rate. We found that when the solution is exchanged with pure water, the frequency shifts back to what is expected for about a monolayer of coverage (see Figure 8). It can be inferred that the first layer formed is

(33) Alexander, S.; Chaikin, P. M.; Grant, P.; Morales, G. J.; Pincus, P. *J. Chem. Phys.* **1984**, *80* (11), 5776–5781.

bound rather strongly to the surface but that subsequent layers are weakly bound, such that they can be washed away by a gentle laminar flow of the pure solvent.

3. *Transition at  $G = 6$ .* The foregoing analysis cannot explain the abrupt transition in the coverage from  $G = 6$  to  $G = 7$  (see Figure 4). If the electrostatic model assumed is correct, then the data indicate that there must be a sharp decrease in effective charge from  $G = 6$  to  $G = 7$ . Such a sharp change could accompany a drastic change in the chemical environment of the dendrimer's surface (amine) groups. There is supportive evidence in the literature for this idea.

de Gennes and Hervet<sup>16</sup> predicted that the "starburst" polymerization of dendrimers can be sustained only up to a limiting generation,  $G_l$ , which they estimated by a self-consistent field calculation. At this limit, a dense packing of surface groups is expected, which could trigger a variety of "surface" property changes. Using their self-consistent method, one finds that the EDA core PAMAM dendrimers used in this work have  $G_l \approx 7$ , exactly where a sudden transition in surface coverage occurs for the case of aqueous solutions. Similarly, in a recent review, Matthews et al.<sup>34</sup> discussed the dense shell issue in terms of a surface crowding factor. Relatively large values of the crowding factor indicate a lack of space for surface groups on the outer shell. For the PAMAM dendrimers used in the present study, one can find that for  $G = 1-6$  the crowding factor discussed is relatively low and nearly constant while from  $G = 7$  and up it increases nearly exponentially with  $G$ . Despite these expectations from theory, at present there is no definitive experimental evidence of drastic structural changes in the PAMAM series at  $G = 6-7$  (see, for example, ref 35).

Nonetheless, the calculations mentioned strongly suggest that, for  $G = 7$ , the surface environment should change drastically from that of lower generations. We conjecture that the observed break in the surface coverage with  $G$  in the present study is a manifestation of this transition, which leads to significantly less net charge per molecule at  $G = 7$ , relative to  $G = 6$  at the conditions of our experiments. A smaller amount of charge per molecule would explain the observed low-frequency shifts for  $G = 7$  through  $G = 9$ , as suggested by eq 8 or 11. Indeed, recent titration data<sup>36</sup> on full generation EDA core PAMAM dendrimers are consistent with this picture. The data indicate the normal response expected for polymers bearing titratable primary amines for  $G = 1$  through  $G = 6$  (i.e. protonation in the range pH 9  $\rightarrow$  6), but an apparent absence of titratable primary amines for  $G = 7$  and  $G = 8$ .

**B. Adsorption from Ethanol.** The important fact about water as solvent in this study is that it promotes protonation of the terminal primary amines of a dendrimer molecule at relatively low pH, giving rise to a positive charge on the polymer. As described, dendrimer multilayers evidently form via the electrostatic interaction between the charge-bearing macromolecules in aqueous solution and their images in the gold electrode. In an organic solvent such as ethanol, with relatively low dielectric constant, primary amines, and therefore PAMAM dendrimers, are not expected to be protonated.<sup>25</sup>

Therefore, multilayer formation via electrostatic interaction is not expected. Indeed, it has been reported<sup>14</sup> that dendrimers adsorbed on gold from ethanolic solution form monolayers with the monolayer thickness increasing rather weakly with generation.

To confirm this difference beyond doubt, we carried out adsorption measurements from ethanolic solution using the same setup as for the aqueous system. Figure 8 shows the  $\Delta f_\infty$  along with values predicted by monolayer models. The equilibrium coverages only slightly exceed the values predicted for monolayers. Clearly, multilayers are not formed, thus supporting the hypothesis that electrostatic interaction is the dominant mechanism of multilayer formation, since it is the one significant difference in interaction forces between the aqueous and ethanolic systems. We also note that the drastic transition in absorbance from  $G = 6$  to  $G = 7$  observed in aqueous solutions does not occur in ethanolic solutions (compare Figures 4 and 8), supporting that this transition is related to a sudden change in the degree of dendrimer protonation in the aqueous system.

#### IV. Conclusions

The adsorption of poly(amidoamine) dendrimers on cleaned gold at room temperature from flowing aqueous solution at pH 6.5–7 and from flowing ethanolic solution has been studied for generations  $G = 1$  through  $G = 9$  by a quartz crystal microbalance technique. We find an exponential growth of the equilibrium surface coverage,  $\Gamma$ , with generation up to  $G = 6$  in aqueous media while in ethanolic solution the growth is much weaker, being roughly linear with  $G$ . The strongly increasing trend of  $\Gamma$  in aqueous media is broken at  $G = 7$ , where an abrupt drop in  $\Gamma$  is observed.

A monolayer model can be used to explain adsorption from ethanolic solution. However, this model cannot describe the data obtained in aqueous solution. In the latter case, the exponential increase of the adsorbed layer thickness for generations  $G \leq 6$  can be described quantitatively by an attractive image-charge interaction of the charged dendrimer molecules with the gold electrode. The break at  $G = 7$  may be a manifestation of "dense-shell" packing which lowers the effective charge on the higher generation dendrimers.

**Acknowledgment.** The authors acknowledge financial support from NSF grant CTS-96-34594 and from NSF MRSEC grant DMR-98-09687.

#### Appendix

Following Alexander et al.,<sup>33</sup> we assume the potential for a macroion in dilute solution is that from the Debye-Hückel (DH) theory, eq 9, but where  $Z^*$  is an effective or renormalized charge per macroion, generally less than the structural charge,  $Z$ , and  $\kappa^{-1}$  is a screening length based on the concentration of counterions from the renormalized macroion charge; eq 10 gives  $\kappa$  when there is no added salt. For dilute macroion solutions, many observable properties are governed by the macroion interactions at relatively large distances, where the pair interaction energy is weak, justifying use of the DH form. This is clearly the case in our use of the potential, where we aim to estimate the distance for the pair interaction energy to just achieve  $kT$ .

For a given number density of macroions,  $c$ , each bearing structural charge  $Z$ , one finds  $Z^*$  and  $\kappa^{-1}$  by matching the long-length-scale predictions of the DH theory with those

(34) Matthews, O. A.; Shipway, A. N.; Stoddard, J. F. *Prog. Polym. Sci.* **1998**, *23*, 1–56.

(35) Prosa, T. J.; Bauer, B. J.; Amis, E. J.; Tomalia, D. A.; Scherrenberg, R. *J. Polym. Sci. Part B—Polym. Phys.* **1997**, *35* (17), 2913–2924.

(36) Thomas, J. L. Columbia University, private communication.

(37) From dendritech literature at <http://www.mmi.org/mmi/dendritech/pamam.html>.

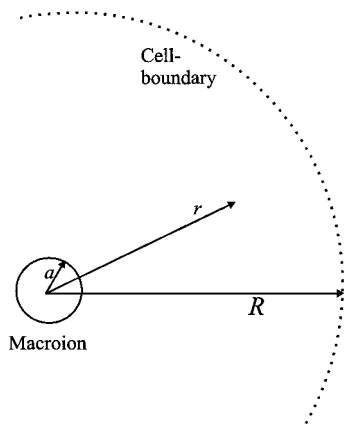


**Figure 9.** Cell geometry for calculation of  $Z^*$  and  $\kappa$ .

of the Poisson–Boltzmann (PB) self-consistent field theory. In particular, the PB equation for the electrostatic potential  $\phi$  is solved in spherical geometry on a “cell” of radius  $R$  concentric with the macroion of radius  $a$  (Figure 9). In our case  $a$  is known from the dendrimer geometry, and  $R$  is determined from  $R = c^{-1/3}$ . The PB equation is

$$-\frac{1}{r^2} \frac{d}{dr} r^2 \frac{d\phi}{dr} = \frac{4\pi}{\epsilon} \rho_0 \exp\left(\frac{-e\phi}{kT}\right); \quad a < r < R \quad (\text{A1})$$

Here,  $\rho_0$  is a normalization constant with units of charge density.  $\rho_0$  and the two integration constants are set to ensure charge neutrality of the cell, expressed by requiring Gauss’s law to be satisfied at  $r = a$

$$-\left[\frac{d\phi}{dr} \epsilon r^2\right]_{r=a} = eZ \quad (\text{A2})$$

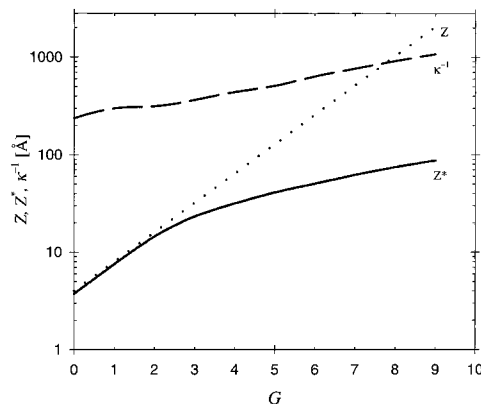


**Figure 10.**  $Z$ ,  $Z^*$ , and  $\kappa^{-1}$  for PAMAM dendrimers  $G = 1$  through  $G = 9$ .

and forcing the potential and the field to vanish at  $r = R$

$$\phi(R) = -\left[\frac{d\phi}{dr}\right]_{r=R} = 0 \quad (\text{A3})$$

The renormalized charge and screening length are then calculated by solving the linearized form of eq A1, obtained by setting  $\exp(-e\phi/kT) \approx 1 - e\phi/kT$  in eq A1, subject to the conditions in eq A3 and with  $\rho_0$  determined from the solution of the PB equation.

Figure 10 shows  $Z$ ,  $Z^*$ , and  $\kappa^{-1}$  for PAMAM dendrimers  $G = 1$  through  $G = 9$  determined by this procedure. The calculation predicts almost no renormalization of charge for lower generations but a significant shift for the more highly charged species. In all cases, the screening lengths greatly exceed the dendrimer radii, by at least an order of magnitude.

LA991283F